Star formation histories in H II galaxies

I. Optical and radio observations

Hans-Jörg Deeg[1,2], **Nebojsa Duric**[2], **and Elias Brinks**[3,4]

[1] Instituto de Astrofisica de Canarias, c/ Via Lactea s/n, E-38200 La Laguna, Canary Islands, Spain
(e-mail: hdeeg@iac.es)
[2] Institute for Astrophysics, Dept. of Physics and Astronomy, University of New Mexico, Albuquerque, NM 87131, USA
(e-mail: duric@phys.unm.edu)
[3] National Radio Astronomy Observatory, P.O. Box O, Socorro, NM 87131, USA (e-mail: ebrinks@andromeda.cimat.mx)
[4] Universidad de Guanajuato, Guanajuato, Gto. 36000, Mexico

Abstract. In this paper we report CCD photometry in broad band B, R, and I colors, as well as in the Hα, for a sample of eight H II galaxies with strong radio emission. In addition, we present new radio continuum observations in the frequency range between 8 and 15 GHz. For seven of these galaxies, previous radio continuum observations have been reported by Deeg et al. (1993); data on Haro 1 are presented here for the first time. Their unusual radio spectra, according to Deeg et al., are a consequence of rapidly changing star formation rates in their past. An independent verification of this conclusion is the motivation for the optical observations reported here. Their interpretation is the subject of the next article in this series. The new radio measurements confirm the interpretation of the radio spectra by Deeg et al. In combination with extinction corrected Hα fluxes, the new radio measurements allow the determination of thermal radio fluxes - a fundamental parameter for star formation rates - with higher reliability than is possible from one wavelength domain alone. Overlays of optical observations at different colors with radio maps, as well as a search of the literature, indicates that all sample galaxies are in interacting environments, which is a possible prerequisite for the strength of the radio emission and star formation observed in these galaxies.

Key words: galaxies: starburst – radio continuum: galaxies – galaxies: interactions

1. Introduction

H II galaxies are actively star forming dwarf galaxies, dominated by one or more giant H II regions. The hot stars which ionize

the H II regions have life times of only a few Myrs, thus the presence of H II regions indicates current or very recent star forming activity on a large scale. The age of a star formation event determines the specific amounts of emission from star forming regions across the electromagnetic spectrum.

In Deeg et al. (1993), – hereafter DBDKS –, radio observations of H II galaxies and their unusual radio continuum spectra were reported and several models for the interpretation of the spectra were introduced. Some of these models allowed estimates of the moment, when major changes in the injection rates of relativistic electrons into the ISM occured. The variations in the injection rate are most likely linked to past changes in the rate of Type II supernovae. To support and verify these models, data at additional wavelengths regimes were obtained. This paper (Paper I) presents a homogeneous set of B, R and I broadband, and Hα narrow band photometry on the eight galaxies, as well as images of them, and discusses their Hα and optical color morphology. An update on more recent radio continuum measurements is given as well. The interpretation of the data presented here is left to the next paper (Deeg, Brinks & Duric 1997, Paper II), where the results from optical and radio observations are integrated into a consistent picture, based on the star formation histories of these galaxies.

Optical broadband colors allow the derivation of independent estimates for the ages of the stellar populations. Whereas a galaxy's emission in the B-band is dominated by brighter main-sequence stars with a lifetime up to about 10^9 yrs, I band emission indicates older stellar disk and Halo (Pop. II) populations. Observations with the B, V and I filters were chosen to cover the widest span of stellar colors. Models quoting $U - B$ versus $B - R$, $B - V$ or $V - K$ colors are frequently used to derive the ages of young stellar populations and the strengths of starbursts (e.g. Krüger et al. 1991; Belfort et al. 1987; Kennicutt 1983; Thuan 1983, 1985; Charlot & Bruzual 1991). U band observations, which were beyond the capabilities of the

equipment available, were taken from the literature for all of the galaxies. The advantage of photometric reductions based on CCD imagery, as undertaken for this work, is the availability of surface photometry, which allows derivation of the local colors of a star forming region. Also undertaken were Hα observations, which yielded morphological information on the size and distribution of the H II regions. The derived Hα flux is used to set lower limits to the thermal radio emission and serves as an indicator for star formation rates in the last few Myrs, as will be discussed in Paper II.

The eight sample galaxies – seven of which were introduced by DBDKS – were selected from the study of blue compact dwarf galaxies by Klein et al. (1991) on the basis of strong radio continuum emission. Haro 1 (= NGC 2415 = UGC 03930 = CGCG 0733.6+3521 = MCG +06-17-021 = CGCG 177−038 = ARK 136) was not included in DBDKS, but was added to this study later, when sufficient radio and optical data became available.

In the following, Sect. 2 covers the optical observations, data reduction, and gives the quantitative results. Additional radio continuum measurements, which improve the frequency coverage in the 8-15 GHz range, are presented in Sect. 3. Section 4 discusses the optical and radio morphology of the galaxies; a summary is given in Sect. 5.

2. Optical data

2.1. The observations

CCD images were obtained at the Capilla Peak Observatory's[1] 0.6 m f/15.1 telescope. The telescope was equipped with a CCD camera with a 320×512 RCA chip (Laubscher et al. 1988), and broadband filters which are closely matched (Beckert and Newberry 1989) to the Johnson UBV (Johnson 1955) and the Kron-Cousins VRI system (Cousins 1976, Bessell 1979). The plate scale of the CCD was 0.658 arcseconds per pixel; the CCD read-out noise was about $80e^-$ per pixel. All galaxy images were taken with a pre-flash, which primes the CCD with about 80 counts/pixel, to suppress a minor nonlinearity of the CCD at low count rates.

The goal was to image all galaxies in the sample through the B, R and I filters, with three exposures of 600 seconds for each filter at photometric conditions. This observing program was completed with a few exceptions, as can be seen in Table 1. The seeing on these images varies between 1.2 and 1.7 arcseconds. Each night, at least two Landolt (1973, 1983) stars were observed several times for intensity calibration and derivation of atmospheric extinction coefficients and color terms. Between each exposure, the telescope was moved by a small fraction of the CCD's field of view in order to position bad columns and hot pixels of the CCD chip at slightly different places on each image.

All of the galaxies were observed at Capilla Peak with an Hα filter set, with filters centered on the Hα emission line (the 'on' filter), and on the nearby continuum (the 'off' filter). The Hα filters at Capilla Peak have a FWHM of about 75Å and are spaced about 80 Å apart. The small overlap of these filters led to worst case transmissivities of slightly over 40% for some galaxies. Some of the galaxies were also imaged at the Kitt Peak[2] 0.9m telescope in its f/7.5 configuration in January 1992, but weather conditions allowed the taking of a few images only. An overview of the Hα observations is given in Table 2. The exposure times given in the table are for either the 'on' or the 'off' filter, which was the same in all cases. When several exposures were taken, 'off' and 'on' filtered exposures were alternated to minimize variations in the airmass and seeing between 'off' and 'on' filtered images. Standard stars for the observations at Capilla were Cyg OB9 #2 and G191 B2B. These two stars are from the list of spectrophotometric standards by Massey et al. (1988) and were selected for the relative absence of spectral features over the wavelengths covered by the Hα filters.

2.2. Broadband data reductions

Image processing was performed using the standard procedures available in the IRAF package. Details of the photometric reductions can be found in Deeg (1992) for the broadband observations and in Deeg (1993) for the Hα observations. Astrometric positions of the galaxy centers were obtained on the B band images with the 'Mann'-measuring engine at the NRAO-AOC in Socorro. These positions were used to create overlays with the radio maps with an accuracy of about 1".

Color terms for the filter-camera system at Capilla Peak were determined from separate observing runs with large numbers of Landolt stars in 1989 and 1991 (Beckert, 1991). Extinction coefficients were fitted for each night based on nightly observations of Landolt stars, using the program 'Photom', written by D. Beckert at the University of New Mexico.

Instrumental magnitudes for each galaxy were determined within a series of elliptical apertures. The ellipses were created by isophotal fitting (Jedrzejewski 1987) to the R band images with the 'ellipse' task in the STSDAS package. The sets of elliptical apertures derived from the R band image (which shows the greatest extent of the galaxies) were then used to obtain the instrumental magnitudes of the galaxies in each filter. Transformation to surface brightnesses allows derivation of the diameter D_{25}, which is the galaxies' major isophotal diameter extending to a surface brightness of 25 m_B arcsec^{-2}. The B band magnitude within that diameter, B_{25}, and the color coefficients $(B-R)_{25}$ and $(R-I)_{25}$ were then obtained. From the same sets of elliptical apertures, the "equivalent" effective diameter D_e^*, as defined in the RC3 (de Vaucouleurs et al., 1991) was derived. The effective aperture is defined as a circular aperture through which passes the flux B_{eff}, which is half of a galaxies' total B band flux. The colors $(B-R)_e$, $(R-I)_e$ and magnitudes B_e within these effective apertures A_e were also obtained.

Table 1. Overview of the broadband observations at Capilla Peak

Name	Date (d.m.y)	Filter	Exp. Time (sec)	Comments
Haro 15	15.10.90	B	3×600	
	"	R	3×600	
	25.10.90	I	3×600	
II Zw 40	12,13.10.90	B	3×600	
	13.10.90	R	3×600	
	"	I	3×600	
Haro 1	14.10.90	B	3×600	
	"	R	3×600	
	15.10.90	I	3×600	
II Zw 70	2.6.92	B	3×400	High altitude cirrus noticed 2 hours
	"	R	3×400	after observation
	"	I	3×400	
Mkn 297	3.5.91	B	3×600	
	"	R	3×600	
	2.5.91	I	600	uncalibrated, missing calibration star
Mkn 314	12.10.90	B	3×600	
	4.10.90	R	3×600	
	"	I	3×600	
Mkn 527	13.10.90	B	3×600	
	"	R	3×600	
	"	I	3×600	
III Zw 102	14,15.10.90	B	300 and 2x 600	
	14.10.90	R	3×600	
	"	I	3×600	

Table 2. Overview of the Hα observations

Name	$V_{\rm rad}$ (km s^{-1})	$\lambda_{\rm H\alpha}$ (Å)	Telescope Ca: Capilla Kp: Kitt Peak	Date (d.m.y)	Exp. Time (sec)	Comments
Haro 15	6414	6703	Ca	23.9.92	3×400	
II Zw 40	800	6580	Kp	13.1.92	1200	
			Ca	23.9.92	3×400	
Haro 1	3782	6646	Kp	13.1.92	1200	
			Ca	3.10.92	3×400	
II Zw 70	1218	6590	Kp	13.1.92	1000	
			Ca	2.6.92	3×400	Missed calibration star, was observed on 26.6.92 for cross calibration
Mkn 297	4707	6666	Kp	13.1.92	1000	
			Ca	23.9.92	400	
Mkn 314	2090	6609	Ca	23.9.92	3×400	
Mkn 527	3540	6641	Ca	23.9.92	3×400	
III Zw 102	1620	6600	Ca	23.9.92	3×400	

Extinction corrections for the color excess from the Galaxy, $E_{\rm g}$, were applied to the measured results, based on the galactic B band extinction $A_{\rm g}$. The RC3 gives values for $A_{\rm g}$ from Burstein and Heiles (1982, 1984). With $E_{\rm g}(V - R) = 0.80E_{\rm g}(B - V)$ (Huchra 1977, Whitford 1958) and $A_{\rm g} = 4.3E_{\rm g}(B - V)$, the extinction correction is $E_{\rm g}(B - R) \approx 0.42A_{\rm g}$ for $B - R$ colors. Similarly, from the average interstellar extinction curve by Savage and Mathis (1979), one obtains for $R - I$ colors: $E_{\rm g}(R - I) = 0.82E_{\rm g}(B - V) \approx 0.19A_{\rm g}$. $A_{\rm g}$ is <0.3 for all galaxies, except for II Zw 40, where the RC3 indicates a large, and uncertain value of $A_{\rm g} = 2.44$.

The internal B band extinction of the galaxies, $A_{\rm i}$, is listed in the RC3 for II Zw 70, Mkn 297, Mkn 527 and III Zw 102. The internal color excesses $E_{\rm i}(B - R)$ and $E_{\rm i}(R - I)$ were derived from $E_{\rm i}(B - V)$ using the relations: $E_{\rm i}(B - R) = 1.80E_{\rm i}(B - V)$ and $E_{\rm i}(R - I) = 0.82E_{\rm i}(B - V)$, which are similar to those derived in the RC2 (de Vaucouleurs, de Vaucouleurs, and Corwin, 1976). $E_{\rm i}(B - V)$ itself was calculated from Eqs. (63) and (64) in the RC3 and depends on the ratio of major to minor diameters, R_{25}, and on the morphological 'T' classification, both taken from the RC3. Our photometric results were not used for the determination of R_{25}, as the ellipse fitting algorithm

could not find the ellipticity reliably for isophotes around the fainter outer parts of the galaxies. The internal color excesses were calculated for those galaxies for which A_i was listed in the RC3. They are rather negligible with $E_i(B-R) \lesssim 0.06$ with the exception of II Zw 70, where $E_i(B-R)$ has an uncertain value of 0.18, due to an uncertain 'T' classification. Internal extinction corrections were not included in the calculation of the corrected color index $(B-R)^\circ$, but are listed separately in Sect. 2.3. No redshift corrections were made to the color indices. The maximum error introduced by this is less than 0.07 mag for the $B-R$ colors, with the exception of Haro 15, where it might be up to 0.15 mag, as this galaxy is more distant than the others. Within the R band lies the Hα emission at $\lambda = 6563$Å, and estimates were made on the fraction of the R band flux which is due to Hα emission. The Hα flux was found to contribute less than 10%, with the exception of II Zw 40, where Hα contributes about 40% to its nucleus' R band flux. Hence, 'Hα corrected' $B-R$ colors of II Zw 40's nucleus would be bluer by about 0.55 mag.

2.3. Broadband results

The morphology of the galaxies is discussed in Sect. 4. Here, the quantitative results of the photometry are given; they are listed in Table 3a. Uncertain values are indicated by colons. The parameters in Table 3a are:

D_{25}, A_e : apparent major isophotal diameter measured at a surface brightness level of $25 m_B$ arcsec^{-2}, and the effective diameter, as introduced in the previous section.
B_{25} : B band magnitude measured within an elliptical aperture with D_{25}.
m'_e : B band surface brightness in magnitudes per square arcsec within the effective aperture A_e.
A_g : Galactic extinction in B band magnitudes, from the RC3.
$E_g(B-R)$: color excess due to extinction in the Milky Way.
$E_i(B-R)$: color excess internal to the sample galaxy.
$(B-R)^\circ_{center}$: $B-R$ color index, corrected for galactic extinction, *not* corrected for internal differential extinction or redshift, within an aperture of about $2''$ size, centered at the maximum of the R band surface brightness ('center'). Several of the galaxies do not have a well defined nucleus; and the color indices at the 'center' indicate a somewhat arbitrary region close to the geometric center of the galaxy; these cases are indicated by parentheses.
$(B-R)^\circ_e$: ditto, within the effective aperture A_e.
$(B-R)^\circ_{25}$: ditto, within an elliptic aperture with major diameter D_{25}.
$(R-I)^\circ_{center}, (R-I)^\circ_e, (R-I)^\circ_{25}$: $R-I$ colors, within the same apertures as the $B-R$ values, corrected for galactic extinction only.

For comparison, Table 3b shows photometric results taken from the literature. Unless indicated, they are all taken from the RC3. The parameters in Table 3b are as follows:

D_{25}, A_e: As in Table 3a.
B_T : Total (asymptotic) B band magnitude
B°_T: Total corrected magnitude. For II Zw 40 it was calculated using the prescriptions in the RC3, Sect. 3.6.d
m'_e: As in Table 3a.
A_g: Galactic extinction in B band magnitudes
R_{25}: The ratio between the major isophotal diameters , D_{25}/d_{25}, measured or reduced to a B-band surface brightness level of 25 mag arcsec^{-2}.
$(U-B)^\circ_e$: $U-B$ color index, corrected for galactic extinction, internal extinction, and redshift, within the effective aperture A_e. The RC3 lists only the uncorrected index $(U-B)_e$; $(U-B)^\circ_e$ was derived using the difference between the corrected and uncorrected total $U-B$ color index which are both given in the RC3, hence: $(U-B)^\circ_e = (U-B)_e + [(U-B)^\circ_T - (U-B)_T]$. The validity of this procedure is indicated in the explanatory Section of the RC3.
$(B-V)^\circ_e$: $B-V$ color index, corrected for galactic extinction, internal extinction and redshift, within effective aperture
$(B-V)^\circ_T$: ditto, total (asymptotic) color index
$(V-R)_e$: $V-R$ color index, not corrected, within effective aperture A_e

The parameters D_{25}, A_e, B_T and m'_e are listed in both tables and are given to allow a direct comparison between the new photometric results and values in the literature. The RC3 was chosen as the preferred reference, as it is the largest and most homogeneous compilation of extragalactic photometric data. The RC3 quotes the B band brightness as the total (asymptotic) magnitude B_T, which can only be obtained by extrapolation from magnitudes at detectable surface brightnesses. Discounting our results for II Zw 40 (its D_{25} is fairly meaningless due to its shape) and II Zw 70 (data taken during poor sky conditions), the offset between B_{25}, measured from the Capilla Peak data, and B_T, from the RC3 is:

$$B_{25} = B_T + (0.11 \pm 0.03) . \tag{1}$$

The small scatter in the offset indicates that the photometry taken at Capilla Peak is reliable and was performed in a consistent fashion; the offset itself is mostly a result of the intrinsic difference between B_{25} and B_T. This difference was included in the derivation of the effective magnitude B_{eff} (which defines A_e) from B_{25} by using: $B_{eff} \approx B_{25} + 0.643$. Whereas the measured values for D_{25} all lie within the error limits given by the RC3, the same cannot be said for the results based on the effective aperture, A_e. The relation given in the RC3 for A_e is valid for normal spiral galaxies only, and the effects of the irregular shapes of the sample galaxies are more pronounced at the smaller diameter A_e than at D_{25}. No systematic offset can be found between $A_{e,Capilla}$ and $A_{e,RC3}$. Using the five galaxies for which A_e is given in the RC3, it is: $A_{e,Capilla} = A_{e,RC3} + (0.1 \pm 1.9)$ arcsec. It should be noted, that A_e in the RC3 has been derived using standard growth curves from measurements at various apertures. For irregular galaxies, the growth curves are certainly not well suited to standardization, and the formal errors quoted in the

Table 3a. Photometry from Capilla Peak observations

Name	Haro 15	II Zw 40	Haro 1	II Zw 70	Mkn 297	Mkn 314	Mkn 527	III Zw 102
D_{25} (arcsec)	62	60:	60	43	66	55	79	96
A_e (arcsec)	16.1	10.1	17.5	7.5	19.9	15.1	32.6	29.7
B_{25}	13.98	15.78	12.88	15.10	13.59	14.24	14.33	12.93
m_e (mag arcsec^{-2})	20.39	21.18	19.48	19.86	20.47	20.52	22.28	20.67
A_g	0.09	2.44:	0.17	0.00	0.11	0.25	0.23	0.07
$E_g(B-R)$	0.04	1.02	0.07	0.00	0.05	0.10	0.10	0.03
$E_i(B-R)$	. . .	. . .	. . .	0.18	0.05	. . .	0.06	0.02
$(B-R)^\circ_{center}$	0.47	-0.01	1.01:	0.50	0.99:	0.84:	1.67	1.54:
$(B-R)^\circ_e$	0.66	0.30	0.84	0.52	0.92	0.81	1.53	1.36
$(B-R)^\circ_{25}$	0.68	0.66	0.87	0.61	0.92	0.86	1.45	1.40
$(R-I)_{center}$	0.73	0.22	0.35:	-0.07	. . .	0.26:	0.65	0.50:
$(R-I)_e$	0.29	-0.49	0.25	-0.02	. . .	0.25	0.62	0.42
$(R-I)_{25}$	0.24	-0.12	0.22	0.16	. . .	0.31	0.64	0.42

Note: Symbols are explained in text.

Table 3b. Photometric results from the literature

Name	Haro 15	II Zw 40	Haro 1	II Zw 70	Mkn 297	Mkn 314	Mkn 527	III Zw 102
D_{25} (arcsec)	51^{+15}_{-11}	. . .	55^{+8}_{-7}	44^{+9}_{-7}	56 ± 5	55 ± 4	85 ± 6	95^{+1}_{-4}
A_e (arcsec)	. . .	12.5 ± 0.9	. . .	. . .	21.3 ± 0.5	13.1 ± 0.3	30.8 ± 0.7	29.4 ± 0
B_T	13.9[1]	$15.48 \pm .13$	$12.78 \pm .13$	$14.83 \pm .13$	$13.44 \pm .13$	$14.13 \pm .13$	$14.24 \pm .10$	$12.83 \pm .13$
B°_T	13.55[1]	13.04:	12.62	14.14	13.41	13.75	13.80	12.70
m'_e (mag arcsec^{-2})	. . .	$21.46 \pm .1$	. . .	. . .	$20.57 \pm .03$	$20.24 \pm .02$	$22.14 \pm .04$	$20.66 \pm .04$
R_{25}	1.38	. . .	1.00	2.88	1.29	1.55	1.35	1.10
$(U-B)^\circ_e$	. . .	-0.39[2]	. . .	. . .	-0.39	-0.35	0.22	0.03
$(U-B)^\circ_T$	-0.40[1]	-0.36[2]	-0.25	-0.79	-0.48	-0.34	0.24	0.13
$(B-V)^\circ_e$	. . .	0.23[3]	. . .	. . .	0.31	0.34	0.79	0.68
$(B-V)^\circ_T$	0.15[1]	0.25[3]	0.35	0.16	0.36	0.38	0.73	0.70
$(V-R)_e$	. . .	. . .	. . .	. . .	0.66[4]	0.63[4]	. . .	. . .

Note: All values from the RC3 except as follows: 1) RC2, not listed in RC3; 2) corrected by $E_g(U-B) = 0.43$ from $(U-B)_e = 0.04$ resp. $(U-B)_T = 0.07$, given in the RC3; 3) corrected by $E_g(B-V) = 0.57$ from $(B-V)_e = 0.80$ resp. $(B-V)_T = 0.82$, given in the RC3; 4) Huchra (1977) lists color indices for several apertures, the one closest to A_e was chosen, not corrected for extinction.

RC3 might be too small. The same argument extends of course to parameters derived from A_e, particularly the surface brightness m'_e. The color indices within the effective apertures are only weakly affected by the uncertainty of A_e, as the color indices do not significantly vary over aperture changes of about 2 arcsecs. The values of the measured colors are not easily verifiable, as independent $B-R$ colors could be found only for two galaxies in Thuan & Martin (1981). No references to colors involving I band measurements could be found in the literature. In the absence of a comparison, the uncertainty of the measured $B-R$ and $R-I$ color indices can only be crudely estimated to be about ± 0.2. As an example of the scatter between published color indices, the compilation by Brosch & Loinger (1991) of $B-V$ colors of III Zw 102 from various sources in the literature is enlightening – differences of 0.5 mag at comparable apertures seem to be common.

2.4. Hα data reduction

The relative wide band of the Hα filters of about 80Å resulted in substantial continuum emission in the Hα images. To remove the continuum emission, a set of 'off' images centered on the nearby continuum was taken. The 'off' images were scaled so that foreground stars in corresponding Hα and 'off' images are of the same brightness. The 'off' image was then subtracted from the Hα image, leaving only the Hα line emission.

The images taken at Capilla Peak were calibrated with images of the spectrophotometric standard stars Cyg OB9 #2 and G191 B2B (Massey et al., 1988), taken through the Hα filter set at various airmasses. Details of the calibration procedure are given in Deeg (1993). The observations taken at Kitt Peak, which were under marginally photometric conditions, were roughly calibrated by observations of I Zw 18 and NGC 2363, which have known Hα fluxes of $3.9 \cdot 10^{-13}$ erg s^{-1} cm^{-2} for I Zw 18 (Davidson et al. 1989, for a square aperture of 20$''$ centered

on the nucleus) and $7.0 \cdot 10^{-12}$ erg s^{--1} cm^{-2} for NGC 2363 (Kennicutt et al. 1980; largest H II region of NGC 2363). The instrumental magnitudes of the reference objects were obtained by using, as closely as possible, the same apertures as given in the literature.

2.5. Results of the Hα observations

Here, only the results of the photometry are derived. Table 4 lists the observed Hα+[N II] fluxes, F_{obs}, and the aperture in which they were measured. Considering the marginal weather conditions during the Kitt Peak observing run and consequent poor internal consistency, the Hα fluxes from the Capilla Peak and the Kitt Peak observations were weighted with a ratio of 4:1. Uncertainties in the flux values are estimated to be about 20%, except for II Zw 70, where the uncertainty is 50%, as none of its observations was under photometric conditions.

To derive the Hα luminosities intrinsic to the emission line regions, the observed Hα+[N II] fluxes are subject to corrections for blending with [N II] line emission, for galactic extinction, and for internal extinction of the emitting H II regions. Corrections for [N II] line blending were taken from [N II]/Hα flux ratios reported in the literature, given in Table 4. If several literature sources quoted different values, averages were taken. The correction for galactic extinction of the emitting Hα line, $A_{g,H\alpha}$, is based on the differential galactic extinction, $E_g(B-V)$, which has been introduced in Sect. 2.2. Based on Caplan and Deharveng (1986) and using the galactic interstellar extinction curve of Savage and Mathis (1979), one obtains for $A_{g,H\alpha}$ in units of magnitude: $A_{g,H\alpha} = 2.50 E_g(B-V)$. The H II regions' internal extinction, A_i, is derived from the measurements of the H_α/H_β Balmer line ratio (Caplan & Deharveng 1986; Brocklehurst 1971; Osterbrock 1989). The values of the line ratio, I(Hα/Hβ), are included in Table 4. This derivation assumes *uniform interstellar extinction* within the H II region; cases with large corrections for internal extinction should therefore only be considered rough estimates, and derived intrinsic Hα fluxes may be valid within a factor of 2 to 3 only. The completely corrected Hα flux is then given by:

$$F_{H\alpha,intr} = F_{H\alpha,obs}(1 + [N \, II]/H\alpha)^{-1} 10^{((Ag+Ai)/2.5)} \, . \qquad (2)$$

Equation (2) was calculated with and without considering the internal extinction A_i. Disregarding A_i should represent a lower limit to the Hα flux densities and is given as $F_{H\alpha,min}$ in Table 4; intrinsic fluxes resulting from the complete correction are given as $F_{H\alpha,intr}$. The table also gives estimates of the sizes of the Hα emitting regions, $D_{H\alpha}$, which were taken from the images presented in Sect. 4.

3. New radio continuum measurements

Since the publication of DBDKS, a number of additional radio continuum measurements, taken at the NRAO-VLA[3], have

been reduced and are summarized here briefly. The data were mostly taken at 8.44 GHz and higher frequencies, with the goal to better determine the thermal radio emission reported in DBDKS. Observations at X (8.44 GHz), U(15.0 GHz) , K(22.4 GHz), as well as additional L (1.49 GHz) band data were undertaken in the C and D-array configurations. An overview of the radio observations and the measured flux densities is given in Table 5. Data already presented in DBDKS are included, this time listing the locations of the flux peak. None of the K band observations produced usable results, due to high atmospheric humidity. Default VLA observing set-ups and standard calibration and mapping procedures were used for all new observations, except for L band, where 8 channel spectral line mode was used to avoid possible external interference. The calibration of the L band data was analogous to the P band observations described in DBDKS. The FWHM of the restoring clean beam has sizes of about $3''$ for X band in C array and $9''$ in D array, $5''$ for U band in D array, and about $50''$ for L band in D array. The new radio data extend the known radio spectra for several of the galaxies, and the new Hα images set limits on the sizes of the H II regions. Where flux densities at similar wavelengths had been determined previously (Table 4 in DBDKS), the new observations generally confirmed these.

We also re-evaluated the inverse Compton loss rates, which are now based on the optical diameter D_{25}, whereas the 1.4 GHz radio diameter was used in DBDKS. This re-evaluation, and the addition of the new radio data, changes the interpretations of the galaxies' radio spectra from DBDKS in minor ways only, except for Haro 15. The bend in its radio spectra is now most likely caused by a 'delta-shaped' relativistic electron injection at a higher age of 6 Myrs, versus 1.2 Myrs previously given. This is due to significantly lower Compton losses from a big difference between its diameter D_{25} of $51''$, and a 1.4 GHz diameter of $16.5''$.

Haro 1 had not been included in DBDKS and high resolution radio data are presented here for the first time. For Mkn 314 the addition of two higher frequency data points made an analysis of its radio spectrum possible. Both galaxies' spectra (Figs. 1a and 1b) can be understood either as combinations of thermal and nonthermal radio emission or as straight power laws. Both possibilities can be fitted to the data with about the same, relatively poor, significance. The numerical results of the fits are given in Table 6a for Haro 1 and Table 6b for Mkn 314. For a description of these tables and of the fits we refer to Table 6 in DBDKS and the associated text.

The additional 8.44 GHz point for Mkn 527 supports the previous interpretation, that its spectrum is a simple sum of thermal and nonthermal powerlaw spectra, and does not change any of the derived parameters. The extension of III Zw 102's spectrum to 14.9 GHz lowers f_{th} to a maximum of 15% and limits the maximum size of the H II region to $3''$, to be compatible with the interpretation involving free-free absorption and emission (fit function I_6 in DBDKS), but this does not change the conclusions in DBDKS otherwise.

Table 4. Hα photometry

Name	Haro 15	II Zw 40	Haro 1	II Zw 70	Mkn 297	Mkn 314	Mkn 527	III Zw 102
Aperture ⊘["]	16.5	19.7	19.7	15.1	23.0	9.9	19.7	19.7
$F_{\mathrm{H}\alpha,\mathrm{obs}}$ $(10^{-13}\mathrm{ergs}^{-1}\mathrm{cm}^{-2})$	6.4	19.5	18	5.1	21	2.8	2.6	9.3
$I([\mathrm{N\,II}]/\mathrm{H}\alpha)$	0.5:[1]	0.025[5]	. . .	0.06[2,7]	0.20[3,7]	. . .	. . .	0.31[7]
$A_{\mathrm{g},\mathrm{H}\alpha}$	0.05	1.42	0.10	0.00	0.06	0.15	0.13	0.04
$F_{\mathrm{H}\alpha,\mathrm{min}}$ $(10^{-13}\mathrm{ergs}^{1}\mathrm{cm}^{-2})$	13	74	20	5.4	28	3.2	2.9	14
$A_{\mathrm{i},\mathrm{H}\alpha}$	0.95	1.13	. . .	0.73	1.13	3.16	. . .	. . .
$I(\mathrm{H}\alpha/\mathrm{H}\beta)$	4.33[6,4]	4.70[5]	. . .	3.9[2,7]	4.7[3,6,7]	11.45:[6,4]	. . .	. . .
$F_{\mathrm{H}\alpha,\mathrm{intr}}$ $(10^{-13}\mathrm{ergs}^{-1}\mathrm{cm}^{-2})$	32	210	. . .	11	79	59:	. . .	. . .
$D_{\mathrm{H}\alpha}$ (arcsec)	1.5	10	3.5	2	3.5	2.5	3.5	5
$D_{\mathrm{H}\alpha}$ (kpc)	0.6	0.5	0.9	0.17	1.1	0.4	0.9	0.6

References in brackets: (1) Denisyuk & Lipovetskii 1984, visual estimates; (2) Osterbrock & Pogge 1987; (3) Kennicutt 1992; (4) Gallagher, Bushouse & Hunter 1989; (5) Terlevich et al. 1991; (6) Mazzarella, Bothun & Boroson 1991; (7) Dahiri 1985
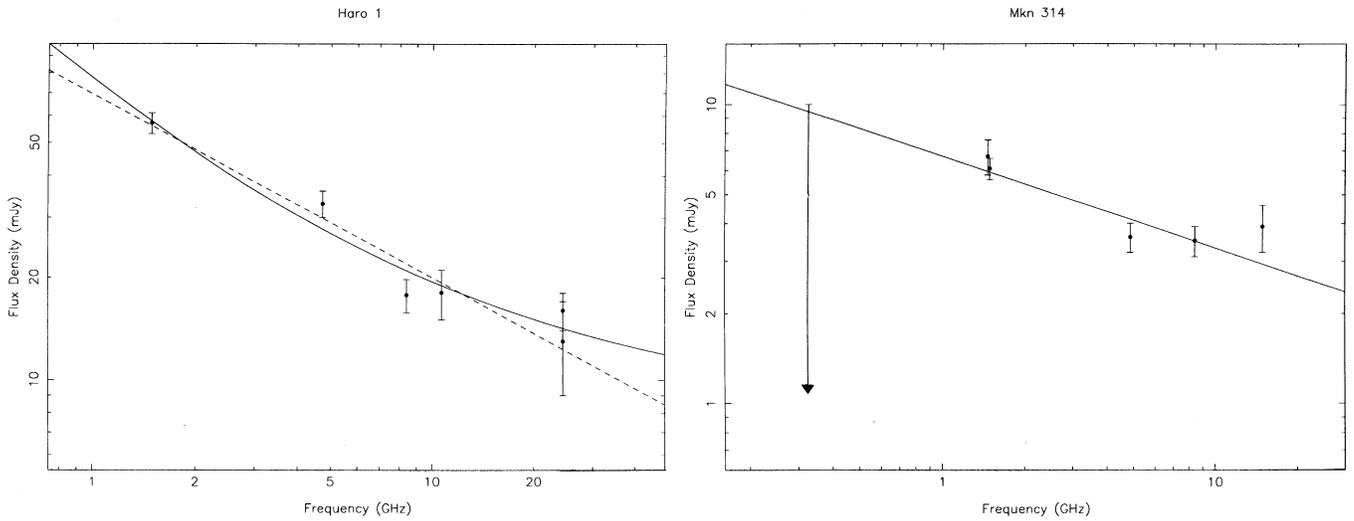
Fig. 1. a Radio spectrum of Haro 1. The solid line is a fit of a combination of thermal and nonthermal power law spectra, the dashed line is a fit of a straight power-law. The data points for 1.489 GHz and 8.44 GHz are from this work, the others are from Klein, Wielebinski and Beck (1984) and Klein et al. (1991). **b** Radio spectrum of Mkn 314. The fit shown is a straight power-law. Data points not listed in Table 5 are from Klein et al. (1991).

3.1. Estimates of the thermal emission

Thermal radio emission serves as a primary indicator for star-forming activity. Thermal radio emission and Hα line emission are both proportional to the intensity of Lyman-continuum photons emitted by hot stars inside the H II region. Although Hα emission is subject to extinction, it can serve as a useful *lower* limit to the thermal radio emission. Radio emission is not subject to extinction or absorption, at least at frequencies $\gtrsim 2$ GHz (DBDKS). Radio measurements at high frequencies ($\gtrsim 8$ GHz) can be assumed to contain very little nonthermal emission and therefore give stringent *upper limits* on the thermal emission, $S_{\mathrm{thR,max}}$, at any frequency. However, the *most probable amount* of thermal radio emission, $S_{\mathrm{thR,fit}}$, (Table 7, for 1.49 GHz) can only be derived from fits of the radio spectra which estimate the thermal fraction, f_{th}, of the total radio emission, S_{totalR} (DB-

DKS, Deeg 1993). A comparison between Hα and thermal radio fluxes is therefore useful. Following Lequeux (1980), the thermal radio flux S_{thR} at a frequency ν and the Hα flux, $F_{\mathrm{H}\alpha}$, are related to each other by:

$$\frac{S_{\mathrm{thR}}(\nu)}{\mathrm{ergcm}^{-2}\mathrm{s}^{-1}} = 1.14 \cdot 10^{-14} \left(\frac{\nu}{\mathrm{GHz}}\right)^{-0.1}$$
$$\times \left(\frac{T_{\mathrm{e}}}{10^{4}\mathrm{K}}\right)^{0.34} \frac{F_{\mathrm{H}\alpha}}{\mathrm{ergcm}^{-2}\mathrm{s}^{-1}} \quad (3)$$

where T_{e} is the electron temperature of the ionized gas, for which a value of 10^{4}K has been assumed. Using the lower limit to the Hα flux, $F_{\mathrm{H}\alpha,\mathrm{min}}$, and the fully corrected flux, $F_{\mathrm{H}\alpha,\mathrm{intr}}$ (from Table 4), the equivalent thermal radio fluxes $S_{\mathrm{thH}\alpha,\mathrm{min}}$ and $S_{\mathrm{thH}\alpha,\mathrm{intr}}$ at 1.49 GHz have been derived (Table 7).

Table 5. Overview of the radio observations

Name	Date	Array Config.	Band	ν (GHz)	S_ν (mJy)	Peak position (1950) α	δ	Comments
Haro 15	28.7.90	B	P	0.325	21.5 ± 2	...		DBDKS
	28.7.90	B	L	1.489	18.5 ± 2	00 46 04.72	-12 59 21.3	DBDKS
	18.4.92	C	X	8.44	5.1 ± 0.6	00 46 04.9	-12 59 20	
	25.9.92	D	U	14.939	4.2 ± 0.6	two peaks discernible, as listed below:		
					2.4 ± 0.5	00 46 04.72	-12 59 24	opt. nucleus
					1.8 ± 0.5	00 46 05.41	-12 59 26	second nucleus
II Zw 40	28.7.90	B	P	0.325	38 ± 4	...		DBDKS
	28.7.90	B	L	1.489	30.5 ± 1.5	05 53 04.92	+03 23 07.0	DBDKS
	21.5.91	D	L	1.489	28.2 ± 1.1	...		
	18.4.92	C	X	8.44	18.7 ± 2	05 53 04.90	+03 23 07.5	
Haro 1	21.5.92	D	L	1.489	54 ± 1	07 33 39.34	+35 21 14.3	
	24.9.92	D	L	1.489	60.2 ± 1.0	07 33 39.52	+35 21 15.3	
	18.4.92	C	X	8.44	17.7 ± 2	07 33 39.39	+35 21 16.0	
double source 85″S	21.5.92	D	L	1.489	13.5 ± 1	07 33 39.3	+35 19 50.5	
	24.9.92	D	L	1.489	17.4 ± 1.0	07 33 39.3	+35 19 52	
	18.4.92	C	X	8.44	9.1	07 33 39.11	+35 19 52.5	
II Zw 70	15.11.91	AnB	P	0.325	12.5 ± 2.5	14 48 55.3	+35 46 47	DBDKS
	19.5.92	C	X	8.44	$\lesssim 2$	...		
Mkn 297	27.7.90	B	P	0.325	244 ± 20	16 03 01.1	+20 40 40	DBDKS
	27.7.90	B	L	1.489	104 ± 7	16 03 1.22	+20 40 40.1	DBDKS
Mkn 314	28.7.90	B	P	0.325	$\lesssim 10$	...		DBDKS
	28.7.90	B	L	1.489	6.1 ± 0.5	23 00 30.63	+16 20 7.88	DBDKS
	16.9.92	D	X	8.44	3.6 ± 0.3	23 00 30.54	+16 20 09.5	
	18.4.92	C	X	8.44	3.4 ± 0.4	23 00 30.54	+16 20 10.0	
	16.9.92	D	U	14.939	3.9 ± 0.7	23 00 30.43	+16 20 08.0	
source 85″ SE	16.9.92	D	L	1.489	42 ± 0.5	23 00 33.4	+16 18 56	
	16.9.92	D	X	8.44	21.7 ± 0.1	23 00 33.35	+16 18 56.8	
	18.4.92	C	X	8.44	23	23 00 33.31	+16 18 57.0	
	16.9.92	D	U	14.939	14.9 ± 0.5	23 00 33.33	+16 18 56.9	
Mkn 527	28.7.90	B	P	0.325	15 ± 4	23 10 40.8	+06 02 58	DBDKS
	28.7.90	B	L	1.489	6.5 ± 0.3	23 10 40.59	+06 02 57.9	DBDKS
	18.4.92	C	X	8.44	3.85 ± 0.4	23 10 40.47	+06 02 58.2	
double src.	18.4.92	C	X	8.44	24	23 10 40.3	+06 01 54	65″S of Mkn 527
III Zw 102	28.7.90	B	P	0.325	68 ± 6	23 18 00.0	+16 57 06.2	DBDKS
	28.7.90	B	L	1.489	46 ± 4	23 17 59.68	+16 57 08.5	DBDKS
	18.4.92	C	X	8.44	17.7 ± 2	23 17 59.7	+16 57 10	
	25.9.92	D	U	14.939	10.5 ± 1.0	23 17 59.6	+16 57 06	

As expected, the fluxes $S_{\mathrm{thH\alpha,min}}$ are significantly lower than the fluxes, $S_{\mathrm{R,fit}}$, which have been derived from fits to the radio spectra (DBDKS; Deeg, 1993). In fact, many authors (e.g. Lequeux (1980), Lequeux et al., (1981), Caplan and Dehaarveng (1986), Berkhuijsen (1983)) *define* the optical absorption in H II regions from the ratio $S_{\mathrm{thH\alpha,min}}/S_{\mathrm{thR}}$. The intrinsic H$\alpha$ emission, $S_{\mathrm{thH\alpha,intr}}$, based on $F_{\mathrm{H\alpha,intr}}$, is about equal or slightly less than $S_{\mathrm{thR,fit}}$, the worst discrepancy is II Zw 70

with $S_{\mathrm{thH\alpha,intr}}/S_{\mathrm{th\,R}} \approx 1/3$. This result agrees with those of the authors just mentioned, who found that even fully corrected Hα fluxes are always approximately equal or less than the Hα-equivalent derived from radio observations. This discrepancy may result from two factors: Although not done in this work, it has been frequent usage to equal the measured total radio flux at 5 GHz with the thermal flux. Unless the radio spectrum of a galaxy is known to be flat, significant nonthermal emission

Table 6a. Results of fits on Haro 1

mechanism	sig.	parameters from fits		
		α		
simple power law	58%	0.54 ± 0.05		
thermal-nonthermal		α	γ_0	$f_{th}[\%]$
separation	59%	0.92 ± 0.30	1.84 ± 0.6	19

Table 6b. Results of fits on Mkn 314

mechanism	sig.	parameters from fits		
		α		
simple power law	68%	0.31 ± 0.06		
thermal-nonthermal		α	γ_0	$f_{th}[\%]$
separation	70%	0.57 ± 0.35	1.14 ± 0.7	43

Note to Table 6a and 6b: For a complete discussion of the table symbols see DBDKS. In short: 'mechanism': type of radio-emission/absorption mechanism that was fitted to the spectrum. A full list is given in DBDKS. Only those mechanisms which gave reasonable fits are given: 'simple powerlaw' from purely nonthermal emission; 'thermal-nonthermal separation' divides the spectrum in the sum of two powerlaws from thermal and nonthermal emission. Parameters from fits: 'sig.': significance of the fit; α: powerlaw-index of the nonthermal radio emission, $S_\nu \approx \nu^{-\alpha}$; γ_0: powerlaw-index of the energy distribution of the electrons at time of injection, $N_0(E) \approx E^{\gamma_0}$; f_{th}: percentage of thermal on the total radio emission at 1 GHz.

**Table 7.** Thermal flux densities at 1.49 GHz, given in mJy

Name	Haro 15	II Zw 40	Haro 1	II Zw 70	Mkn 297	Mkn 314	Mkn 527	III Zw 102
$S_{totalRad,1.49GHz}$	23 ± 4	30.5 ± 2	57 ± 3	4.6 ± 0.8	104 ± 7	6.4 ± 1	6.5 ± 0.5	49 ± 5
$S_{thR,fit}$	1.3	22	14	3.4	2.7	3.0	3.9	6.1
$S_{thR,max}$	4.3	25	18	3.6	20	4.1	3.4	9.0
$S_{thH\alpha,min}$	1.4	8.0	2.1	0.55	3.1	0.38	0.29	1.5
$S_{thH\alpha,intrinsic}$	3.5	23	. . .	1.2	8.8	6.4	. . .	. . .
S_{thUV}	5.6	. . .	13.5	. . .	. . .	. . .	. . .	. . .
$S_{th,adopt}$	3.5 ± 2.2	23 ± 3	15 ± 2	3.2 ± 0.5	6.8 ± 4.1	3.2 ± 0.7	3.9 ± 0.4	6.1 ± 3.0
$f_{th,adopt,1.49GHz}$	$0.15 \pm .09$	$0.75 \pm .1$	$0.26 \pm .04$	$0.7 \pm .1$	$0.07 \pm .04$	$0.5 \pm .1$	$0.6 \pm .06$	$0.12 \pm .06$

Notes: $S_{totalRad,1.49GHz}$ is an averaged value from the values given in Paper I and DBDKS. As the radio emission from Haro 15 has some absorption at 1.49 GHz, its intrinsic flux density has been estimated from measurements at higher frequencies.
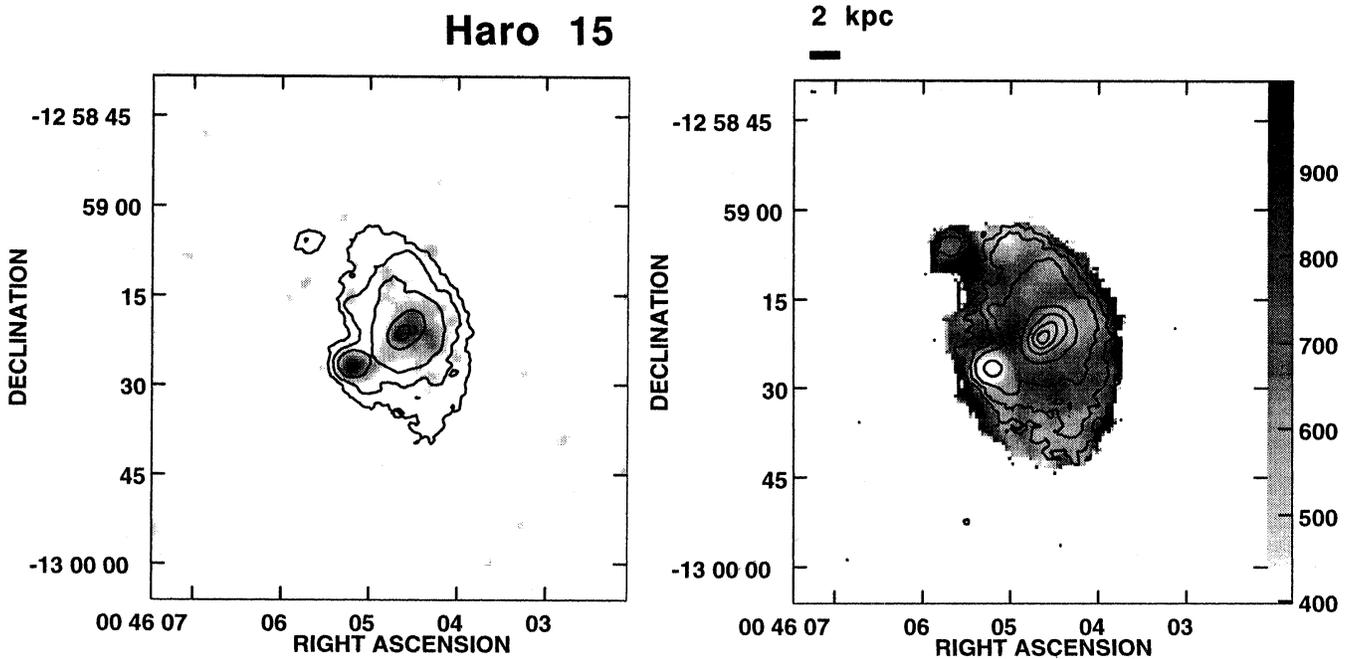
Fig. 2. a Haro 15. Hα brightness (greyscale) versus B band (contours). **b** Haro 15. $B - R$ colors (greyscale) versus B band surface brightness (contours). In all frames with $B - R$ colors in Figs. 2–8, the calibration of the $B - R$ colors in millimag is indicated in the greyscale on the right side.
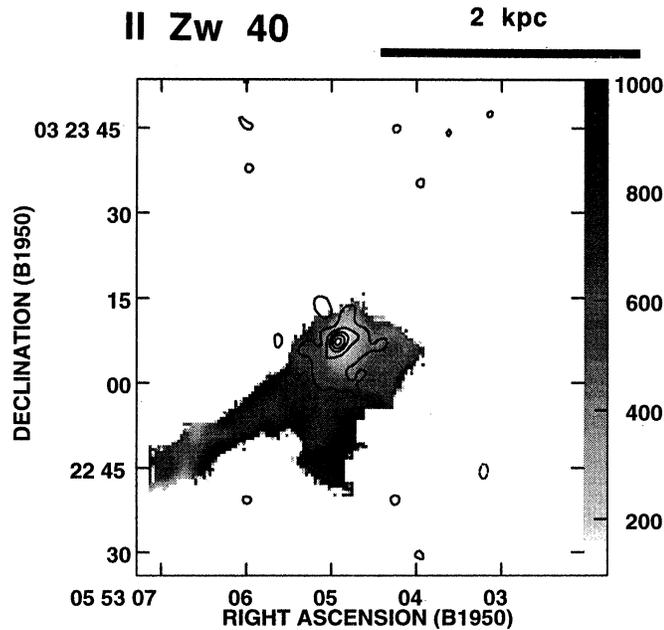
Fig. 3. II Zw 40. $B - R$ colors (greyscale) versus 8.44 GHz X Band (contours). The Peak flux density is 5.32 mJy/Beam, with a beam FWHM of $3''$. The contour lines are at fractions of -0.1, 0.1, 0.3, 0.5, 0.7, 0.9 of the peak flux density (dotted contours are 'negative flux density' artefacts from processing).

may still be present at 5 GHz and the thermal radio flux quoted from such a measurement is too large. Second, the corrections to obtain the intrinsic Hα fluxes may be poor, as the Hα flux may be subject to absorption that deviates from the conditions of uniform interstellar absorption and from the galactic extinction laws.

For the galaxies Haro 1 and Haro 15, Fanelli et al. (1988) performed spectral synthesis based on UV spectra. The UV spectra contain direct information on the intensity of ionizing photons in the H II regions, which Fanelli et al. used to derive a thermal radio flux density at 5 GHz, S_{thUV}, for which a conversion to 1.49 GHz is included in Table 7. In the case of Haro 1, S_{thUV} agrees well with the measured radio flux, whereas for Haro 15, S_{thUV} is barely compatible with $S_{\mathrm{R,max}}$. For the adopted thermal flux, $S_{\mathrm{th,adopt}}$, and the adopted thermal fraction $f_{\mathrm{th,1.49GHz}}$, the largest weight was given to the radio spectra if either free-free absorption or thermal-nonthermal separation gave good fits in DBDKS, otherwise all estimates were given about equal weight. These adopted values are used in the discussion of Paper II.

4. Morphology of the individual galaxies

Optical B band and 1.49 GHz radio contour overlays for six of the eight galaxies have been shown in DBDKS. In this Section we discuss the morphology of the galaxies based on these im-

ages of DBDKS, on the additional overlays shown here, and on a literature search using NED[4]

$B - R$ color images were created by taking the logarithm of the ratio of the B- and R- images, with appropriate calibration constants added. The images are corrected for the galactic color excess, as discussed in the section on photometry. The greylevels of the images are therefore representative of calibrated $B - R$ surface color values. The $B - R$ images were smoothed with a Gaussian kernel of $4''$ FWHM and have an approximate cutoff at a surface brightness of 23 mag/(arcsec)^2 in B and R band. 'Blue' regions ($B - R$ small) are light and redder regions are dark.

If available, Hα images taken with the Kitt Peak 0.9m telescope are shown. The count rates of the Hα images taken with the 0.6m at Capilla Peak are very low, on the order of 10–20 counts per pixel at the maximum of the Hα emission, which accounts for the clearly visible background noise. For some of the galaxies, overlays of optical images with new X band (8.44 GHz) radio maps are shown; for L band (1.49 GHz) radio maps, the reader is referred to DBDKS.

4.1. Haro 15

Mazzarella et al. (1991) classify Haro 15 as a "strongly interacting separated galaxy or a single highly perturbed system which may be an advanced merger". The secondary nucleus has stronger Hα emission (Fig. 2a) than the main nucleus. This is also reflected in U band radio measurements, which at 14.9 GHz are mostly thermal emission, where the secondary nucleus is brighter than the central nucleus. The radio emission from it has a much flatter spectral index than the central nucleus and probably a larger fraction of thermal emission, possibly indicating a very young star forming region. This is also supported by the blue color ($B - R \approx 0.4$) of the secondary nucleus within the fairly uniform colors of the disk (Fig. 2b).

4.2. II Zw 40

II Zw 40 has long been known as a prototypical H II galaxy or BCDG, i.e. a Blue Compact Dwarf Galaxy (Sargent and Searle, 1970). The nucleus of II Zw 40 is dominated by one large H II region, with a diameter of about 0.5 kpc, and the radio emission is centered on the nucleus at all frequencies. As mentioned previously, II Zw 40's Hα emission is so strong, that it contributes 40% to the R Band flux at the nucleus. This indicates a starburst of extraordinary strength, as is also evident from the colors of the nucleus, which are much bluer than those of the southern and south-eastern extensions (Fig. 3). Although only one large, featureless H II region is seen, H I observations (Brinks and Klein, 1988) revealed two kinematically separate systems, interpreted as two interacting H I clouds with approximately equal mass, of which only the northern cloud has an optical counterpart in II Zw 40. This indicates an H I mass an order of magnitude larger than

---

[4]   The NASA/IPAC extragalactic database (NED) is operated by the Jet Propulsion Laboratory, California Institute of Technology, under contract with the National Aeronautics and Space Administration.
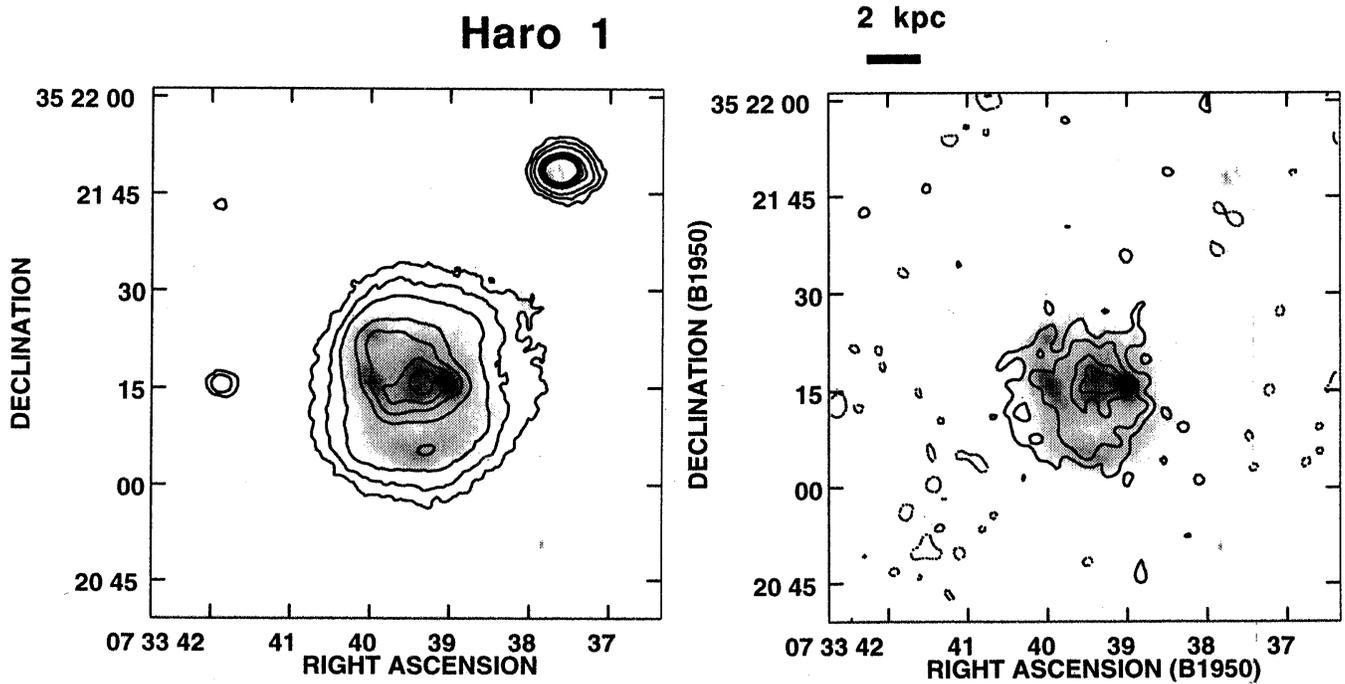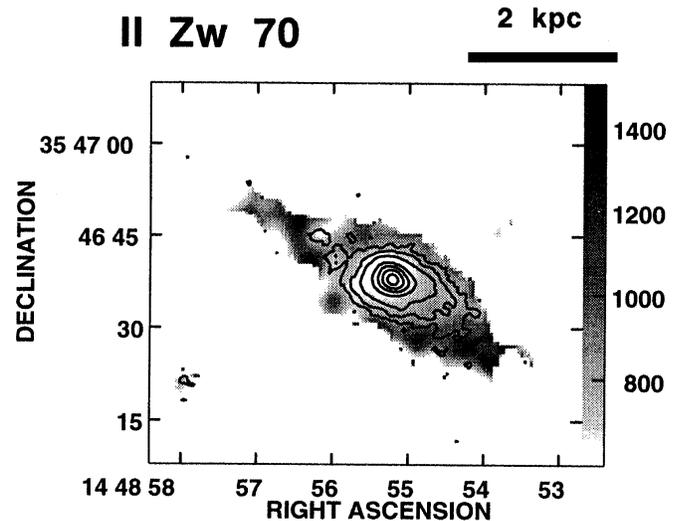
Haro 1

Fig. 4. a Haro 1. Hα brightness (greyscale) versus B band (contours). **b** Haro 1. Hα brightness (greyscale) versus 8.44 GHz X band (contours). The Peak flux density is 1.13 mJy/Beam, with a beam FWHM of 3″. The contour lines are at fractions of -0.2, 0.2, 0.4, 0.6, 0.8 of the peak flux density.

the visible mass. Based on the H I mass of the northern cloud, Sage et al. (1992) find an unusual star formation efficiency[5] for II Zw 40, which might be the result of the rare event of a merger between two gas-rich dwarf galaxies, being observed at the peak of its star forming episode. They call II Zw 40 "one of the most extreme galaxies known". This result is also supported by FIR observations (Joy & Lester 1988).

4.3. Haro 1

Haro 1 is described (Schneider and Salpeter, 1992) as a paired galaxy with little or no tidal disturbance. Its companion is UGC 3937, with a redshift difference of $\Delta v = 210\,\mathrm{km\,s^{-1}}$ and a linear separation of 350 kpc. Van der Burg (1985) reports on a possible detection of a third companion in H I at $07^{\mathrm{h}}\,33^{\mathrm{m}}\,54^{\mathrm{s}}$, $+35°46′$. The B-band image (Fig. 4a), reveals a large irregular nucleus, whereas in Hα, at least 6 distinct clumps are discernible. The X-band map (Fig. 4b) shows the radio emission to be peaked at the second and third strongest H II regions near the center of the disk and the eastern and southern H II regions can be seen as local maxima of the radio emission. The galaxy's star forming regions appear to suffer high extinction, as its $B - R$

---

[5] Sage et al (1992) note that the star formation rate for star forming dwarf Irregulars is generally higher than in starforming ellipticals, but not the starforming efficiency(SFE). This makes II Zw 40 an unusual case. The SFE is defined as the ratio between the mass which is converted into newly formed stars and the entire mass of the starforming region.

II Zw 70

Fig. 5. II Zw 70. $B - R$ colors (greyscale) versus B band (contours).

color of 0.85 ± 0.03 is very uniform and gives no suggestion of concentrated starforming activity.

4.4. II Zw 70

II Zw 70 has been included in the "Atlas and Catalogue of Interacting Galaxies" by Vorontsov-Vel'yaminov (1959, 1977). Together with II Zw 71 (UGC 5962 =VV 324a) at a projected distance of 46 kpc, Dahiri (1985) classifies them as "two Sa spirals, far apart, with signs of interaction". Lake & Schom-

mer (1984) derive a ratio of total-to- visible mass for the II Zw 70/71 system of 19 ± 5 from orbital analysis. This is somewhat higher than that derived from H I observations by Balkowski et al. (1978) of 5 and 14 for II Zw 70 and II Zw 71. Besides being classified as a "genuine BCDG" by Skillman and Klein (1988), II Zw 70 appears to be a distorted spiral (Fig. 5) with the nucleus being its distinctively bluest region. The same authors also speculate on the presence of a radio supernova, based on the very steep nonthermal spectral index. Unfortunately, no useful radio maps of this galaxy could be obtained in the course of this work, but the position derived from 6 cm VLA C-array observations by Wynn-Williams and Becklin (1986) agrees well with the nucleus as seen in optical broad- band and Hα emission.

4.5. Mkn 297

Mkn 297 is an unusual galaxy in several respects. Its optical morphology, especially in Hα, is dominated by a large number of clumpy features (see Fig. 5 in DBDKS) and contains a possible radio supernova (Lonsdale et al., 1992; DBDKS and references therein). Saakyan and Khachikyan (1975) included Mkn 297 in their list of super associations of H II regions. Vorontsov-Velyaminov (1977) classifies it among tight interacting systems, as "coalescent galaxies and a chain of 3 dwarfs". Meahara et al. (1988) define 20 clumps in Mkn 297, on which they provide detailed photometry. Alloin and Duflot (1979) interpret Mkn 297 as the collision of two late spirals, and Taniguchi & Noguchi (1991) report on numerical N-body simulations of the collision of two disk galaxies; the results of their simulations are overlaid onto an optical image of Mkn 297. The interpretation of Mkn 297 as the merger of two disk galaxies is inconsistent with the findings by Burenkov (1988), who concludes from spectroscopic observations that the abundance gradients of nitrogen and oxygen are only consistent with *one* spiral galaxy; the second galaxy is probably an irregular.

4.6. Mkn 314

Mkn 314 (= NGC7468 = UGC 12329 = CGCG 453$-$052 = CGCG 2300.5+1620) is considered a possible polar ring galaxy by Whitmore et al. (1990), with the polar rings being the outer extensions at the northern and southern end, visible in the contour lines of the B-band image (Fig. 6). The galaxy has at least two optical nuclei distributed along a line in the NNE-SSW direction of which only the northernmost one has significant Hα emission.

4.7. Mkn 527

Mkn 527 is a spiral galaxy, classified as SAB(r)a; with the bars (Fig. 7) extending from the nucleus in the SE and NW directions, and an outer ring in the plane of the disk. As a member of the Pegasus cluster it appears in several publications related to cluster galaxies (e.g. Cornell et. al 1987, Giovanelli & Haynes, 1985). Its Hα emission is centered on the nucleus. Nuclear starforming activity is not reflected in the surface colors, in which Mkn 527 appears like a normal spiral galaxy.
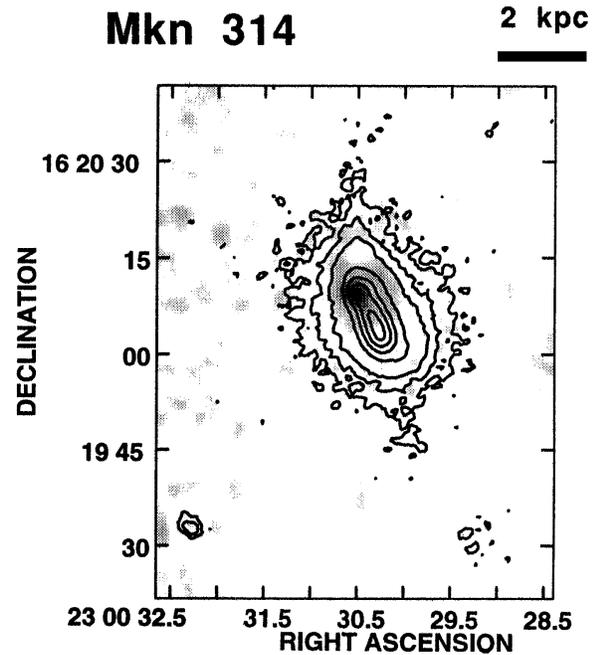

Fig. 6. Mkn 314. Hα brightness (greyscale) versus B band (contours).
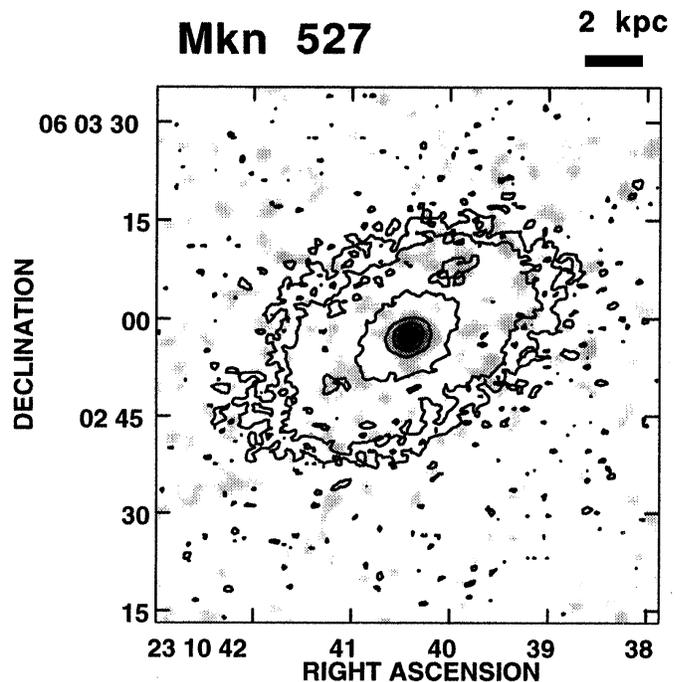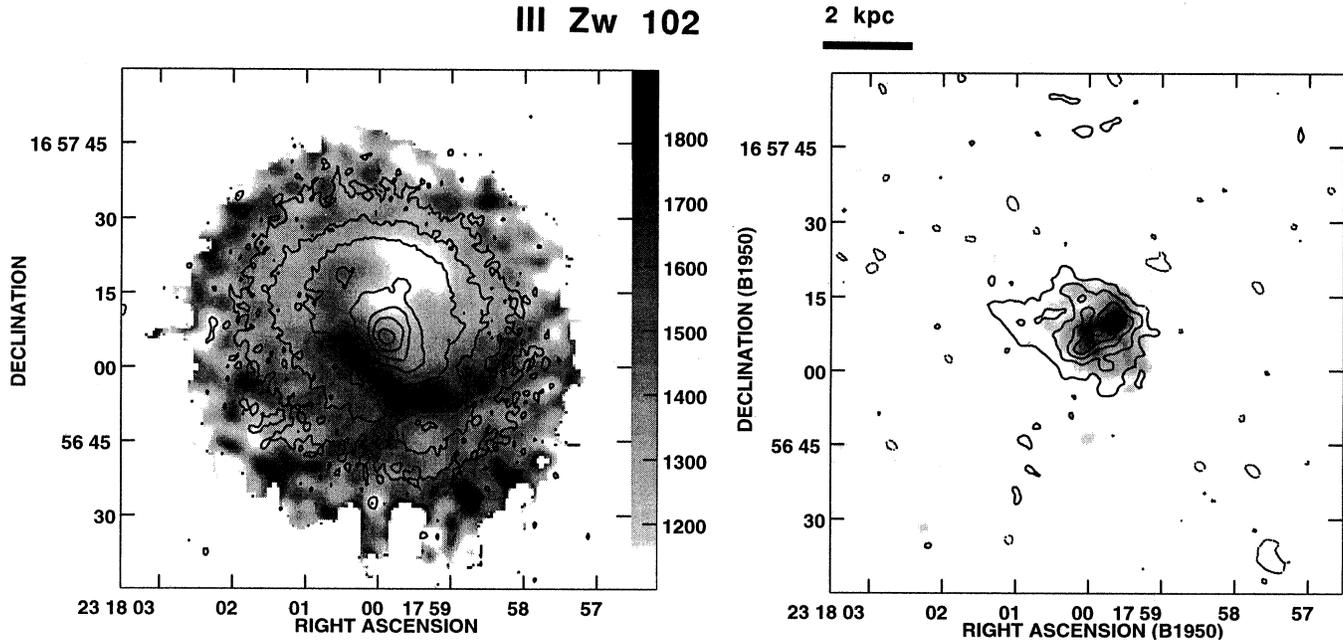

Fig. 7. Mkn 527. Hα brightness (greyscale) versus B band (contours).

4.8. III Zw 102

Whitmore et al. (1990) consider III Zw 102 as 'related to polar-ring galaxies'; with its dust lanes being similar to polar rings without the luminosity. Various catalogs and publications classify III Zw 102 among elliptical, Sa or S0 galaxies; most mention its peculiarity. Brosch and Loinger (1991) note that III Zw 102's common classification among BCDGs is apparently the result of

Fig. 8. a III Zw 102. $B - R$ colors (greyscale) versus B band (contours). **b** III Zw 102. Hα brightness (greyscale) versus 8.44 GHz X Band (contours). The Peak flux density is 1.16 mJy/Beam, with a beam FWHM of $3''$. The contour lines are at increments of 10% the peak flux density.

its selection among the 115 BCDGs of Thuan & Martin (1981), as its diameter of 13 kpc hardly classifies it as a dwarf. Brosch and Loinger (1991) perform extensive modeling of III Zw 102's internal extinction. Although the brightness profile of the underlying disk agrees well with a fit to the de Vaucouleurs $r^{1/4}$ law which indicates elliptical structure, they are unable to decide on its morphology. The colors of the disk are probably dominated by variations in the dust extinction (Fig. 8a). The elongated reddish extinction feature in the NE to SW direction near the center also appears prominently in the models of III Zw 102's extinction by Brosch and Loinger. The radio-emission (Fig. 8b) traces the Hα emission quite well, implying that at least in the area of the Hα emission, optical extinction cannot be very large. The radio emission does not reflect the extent of the dust envelope (Fig. 1f in DBDKS).

5. Concluding remarks and summary

With this paper primarily presenting new data, and Paper II containing a discussion of both the optical and radio results, only some concluding remarks will be given.

– A homogeneous set of observations of a sample of H II galaxies through B, R and I filters was obtained. The photometric results consist of integrated magnitudes, surface brightnesses, effective and D_{25} diameters, and extinction corrected colors at the galaxies' centers and within the aforementioned diameters. Whereas the magnitudes and D_{25} agree well with previously published data, discrepancies in the effective diameter A_e can be attributed to the strong influence of a galaxy's irregular mor-

phology on the brightness distribution within smaller diameters. The B and R filtered CCD images were used to construct images depicting the $B - R$ colors across the surface of the galaxies.

– Results from flux calibrated Hα imagery are presented. Hα fluxes were corrected for extinction and N II-Hα line blending when possible. Whereas uncorrected Hα fluxes give *lower limits* to the thermal radio emission of the galaxies, the corrected Hα fluxes allow an estimate of the *probable* thermal radio fluxes, independent from radio measurements. These estimates agree well with thermal radio fluxes derived from actual radio data.

– New radio measurements give nearly complete frequency coverage of the sample galaxies in the range of 0.32 to 15 GHz. The addition of high frequency measurements allows more stringent limits to be set to the thermal emission of some of the galaxies, but did not change significantly DBDKS's interpretation of their radio spectra. The new data allowed to analyze the radio spectra of two additional galaxies in a fashion similar to DBDKS. These spectra, however, did not lend themselves to good fits and an unambiguous interpretation.

– Comparison of the $B - R$ color maps, the radio maps and the Hα images show that in some galaxies, such as II Zw 40, there is a clear spatial correlation between all indicators of star formation, including radio emission, H II regions and areas of blue stellar colors. Whereas the 1.4 GHz, or 8.44 GHz, radio morphology generally agrees well with the Hα emission, there is suffient extinction in some galaxies, such as Mkn 297, to obscure the expected blue colors from the star forming regions.

– Despite the fact that the galaxy sample is not particularly rigorously defined, it is interesting to note, that (with the exception of Mkn 527, which does not fit the description of H II galaxies very well) all sample galaxies have been interpreted by at least one author as merging or an interacting systems. The sample galaxies were selected for their strong radio-continuum emission from a larger set of H II galaxies. Possibly, only the relatively short lived merger/interaction events allow for the temporarily increased star formation rates and a correspondingly high radio emission, high enough that they were selected for this study from the much larger pool of H II galaxies.

References

Alloin, D., Duflot, R.,1979, A&A 78, L5

Balkowski, C., Chamaraux, P., Weliachew, L., 1978, A&A 69, 263

Beckert, D.C., 1991, unpublished data

Beckert, D.C, Newberry, M.V., 1989, PASP 101, 849

Belfort, P., Mochkovitch, R., Dennefeld, M., 1987, A&A 176

Berkhuijsen, E.M., 1983, A&A 127, 395

Bessell, M.S., 1979, PASP 91, 597

Brinks, E., Klein, U.,1988, MNRAS 231, 63p

Brocklehurst, M., 1971, MNRAS 153, 471

Brosch, N., Loinger, F., 1991, A&A 249, 327

Burenkov, A.N., 1988, Afz 28, 47

Burstein, D., Heiles, C., 1982, AJ 87, 1165

Caplan, J., Deharveng, L.,1986, A&A 155, 297

Charlot, S., Bruzual, G., 1991, ApJ 367, 126

Cornell, M.E., Aaronson, M., Bothun, G., Mould, J., 1987, ApJS 64, 507

Cousins, A.W.J., 1976, Mon. Notes Astr. Soc. S. Afr. 37, 8

Dahari, O., 1985, ApJS 57, 643

Davidson, K, Kinman, T.D., Friedman, S.D., 1989, AJ 97, 1591

Deeg, H.J., 1992, "Reduction and Photometry of Multi-Color Galaxy Observations", Documentation of the Capilla Peak Observatory, The University of New Mexico, Albuquerque

Deeg, H.J., 1993, PhD. Thesis, The University of New Mexico

Deeg, H.J., Brinks, E., Duric, N., 1997, submitted (Paper II)

Deeg, H.J, Brinks, E., Duric, N., Klein, U., Skillman, E., 1993, ApJ 410, 626 (DBDKS)

de Vaucouleurs, G., de Vaucouleurs, A., Corwin., 1976, Second reference catalog of bright galaxies (RC2) (Austin, Univ. of Texas Press)

de Vaucouleurs, G., de Vaucouleurs, A., Corwin, H.G., et al., 1991, Third reference catalog of bright galaxies (RC3) (New York, Springer Verlag)

Fanelli , M.N., O'Connell, R.W., Thuan, T.X., 1988, ApJ 334, 665

Giovanelli, R., Haynes, M.P., 1985, ApJ 292, 404

Huchra, J.P., 1977, ApJS 35, 171

Jedrzejewski, R.I., 1987, MNRAS 226, 747

Johnson, H.L. 1955, Ann. d'Ap. 18,4, 292

Joy, M., Lester, D.F.,1988, ApJ 331, 145

Kennicutt, R.,1983, ApJ 272, 54

Kennicutt, R., Balick, B., Heckman, T., 1980, PASP 92, 134,

Klein, U., Weiland, H., Brinks, E., 1991, A&A 246, 323

Klein, U., Wielebinski, R., Beck, R., 1984, A&A 133, 19

Krüger, H., Fritze-von Alvensleben, U., Loose, H.-H., Fricke, K.J., 1991, A&A 242, 343

Lake, G., Schommer, R.A.,1984, ApJ 279, L19

Landolt, A.U., 1983, AJ 88, 439

Landolt, A.U., 1973, AJ 78, 959,

Laubscher, B.E., Gregory, S., Bauer, T.J., Zeilik, M., Burns, J.O., 1988, PASP 100, 131

Lequeux, J.,1980, in Star Formation (Saas-Fee, Geneva Obs), p. 75

Lequeux, J., Maucherat-Joubert, M., Deharveng,J.M., Kunth, D., 1981, A&A 103, 305

Lonsdale, C.J., Lonsdale, C.J., Smith, H.E.,1992, ApJ 391, 629

Massey, P., Strobel, K., Barnes, J.V., Anderson, E., 1988, ApJ 328, 315

Mazzarella, J.E., Bothun, G.D., Boroson, T.A., 1991, AJ 101, 2034,

Maehara, H., Hamabe, M., Bottinelli, L., et al., 1988, PASJ 40, 47

Osterbrock, D.E., 1989, Astrophysics of Gaseous Nebulae and Active Galactic Nuclei (University Science Books, Mill Valley, California)

Saakyan, K.A., Khachikyan,É.E., 1975, Astrofizika 11, 207,

Sage, L.J., Salzer, J.J., Loose, H.-H., Henkel, C., 1992, A&A 265, 19

Sargent , W.L.W., Searle, L., 1970, ApJ 162, L155

Savage, B.D., Mathis, J.S.,1979, ARA&A 17, 73

Schneider, S.E., Salpeter, E.E., 1992, ApJ 385, 32

Skillman, E.D., Klein, U., 1988, A&A 199, 61

Taniguchi, Y., Noguchi, M., 1991, AJ 101, 1601

Thuan, T.X., 1983, ApJ 268, 667

Thuan, T.X., 1985, ApJ 299, 881

Thuan, T.X., Martin , G.E., 1981, ApJ 247, 823

van der Burg, G.,1985, A&AS 62, 147

Vorontsov-Velyaminov, B.A.,1977, A&AS 28, 1

Whitmore, B.C., Lucas, R.A., McElroy, D.B., et al., 1990, AJ 100, 1489

Wynn-Williams, C.G., Becklin, E.E., 1986, ApJ 308, 620